**Dynamic Control of Nanoparticle Assembly Using Solid-Binding Proteins**

Yifeng Cai

A thesis

submitted in partial fulfillment of the requirements for the degree of

Master of Science in Chemical Engineering

University of Washington 2021

Committee:

François Baneyx

Lilo Pozzo

Program Authorized to Offer Degree:

Department of Chemical Engineering

University of Washington

## Abstract

Dynamic Control of Nanoparticle Assembly Using Solid-Binding Proteins

Yifeng Cai

Chair of the Supervisory Committee: François Baneyx
Department of Chemical Engineering

Solid binding peptides (SBPs) are short sequences of amino acids selected by combinatorial techniques for their ability to bind to inorganic or synthetic surfaces. SBPs can be genetically encoded within the framework of larger polypeptides to produce solid-binding proteins that retain biological function while gaining the ability to organize inorganic components into hybrid materials. In this project, we build on previous efforts showing that derivatives of superfolder green fluorescent protein (sfGFP) fitted with oppositely located Car9 silica-binding peptides drive repeated cycles of silica nanoparticle assembly and disassembly when the solution pH is toggled between 7.5 and 8.5. We explore how aggregate size is influenced by the substitution of two lysine residues in the Car9 sequence by alanaine, and how the location of the mutant sequence on the sfGFP framework, the solution pH, and the chemical fatigue associated with the accumulation of sodium ions upon alkalinization, impact colloid formation and dispersion. Furthermore, we describe progress in the construction, expression and purification of *de novo* designed trimeric and tetrameric proteins modified with a Car9 extension which might prove useful to organize silica nanoparticles into defined architectures.

## Table of Contents

**Abstract** ..... 3

**Chapter1. Introduction** ..... 7

**1.1 Assembly of hybrid nanomaterials** ..... 8

**1.2 Solid binding peptides and Car9** ..... 10

**1.3 Silica surface chemistry and the absorption of peptides and proteins to silica nanoparticles** ..... 13

**Chapter2. The sfGFP-SiNP system** ..... 15

**2.1 Introduction** ..... 15

**2.2 Materials and Methods** ..... 17

**2.2.1 DNA manipulations and protein purification** ..... 17

**2.2.2 pH cycling for protein-NP solutions** ..... 17

**2.2.3 Dynamic Light Scattering.** ..... 18

**2.3 Results and Discussion** ..... 18

**2.3.1 Chemical control of colloidal assembly with bifunctional solid-binding proteins: influence of SBP sequence and insertion location** ..... 18

**2.3.2 Controlling protein-NP aggregate size by modulating solution conditions.** ..... 21

**2.4 Conclusions and future direction** ..... 26

**Chapter3. *De novo* designed proteins** ..... 28

**3.1 Introduction** ..... 28

**3.2 Materials and Methods** ..... 29

**3.2.1 DNA manipulations and protein purification ..... 29**

**3.2.2 Assembly of protein-NP solutions ..... 30**

**3.3 Results and Discussion ..... 30**

**3.3.1 Protein tagging and purification ..... 30**

**3.3.2 Attempted assembly of Ni-NTA AuNP using Ank1C4-His ..... 32**

**3.4 Conclusions and future direction ..... 33**

**References ..... 34**

**Appendix ..... 40**

## Acknowledgement

There are plenty of people I would like to thank for supporting me over the last two years: my advisor, François Baneyx, for guiding and encouraging me during my work, my lab-mates, Nada, Jinrong, and Karthik, for their camaraderie and patience, my graduate student advisor, Allison, and my friends and colleagues in the department for providing me great ideas. I also want to thank my family for their love and strong support. They encouraged me throughout the entire master program study and inspired me to always look forward. Additionally, I would like to thank my friends, Renyu, Jinge, and Jianing, for supporting me though the most difficult of times and lead me to a broader and brighter future.

## Chapter1. Introduction

Materials that exhibit ordered structures at the nanoscale and beyond often possess unique mechanical, colloidal, electronic, and optical properties that can be harnessed for the design of novel engineering systems or sensors.[1–3] For example, multi-dimensional assembly of gold nanoparticles with controlled morphology into highly ordered arrays, long chains and sheets has been constructed for the synthesis of composite nanomaterials and the unique applications in sensing and memory devices.[4] Traditionally, the approaches to nanomaterial fabrication are achieved through ‘top down’ techniques such as lithography, milling or electrospinning, as well as via "bottom up" techniques such as chemical vapor deposition (CVD) and electrodeposition through templates, or self-assembly.[5] While decades of nanotechnology research have delivered promising advances in nanoparticle and nanostructure synthesis,[6,7] the production of ordered assemblies and the dynamic control of their structure remain difficult and inefficient.[2,3]

In recent years, significant efforts have been directed at developing self-assembly methodologies for precision nanofabrication of static and dynamic structures[8–11] that may prove useful in addressing challenges in energy storage, opto-electronics and catalysis.[12,13] Remarkably, many of these challenges have already been solved by organisms which uses proteins, peptides as building blocks and scaffolds for the construction of complex functional architectures.[1,14] Insights obtained in the traditional field of biomimetics have been supplemented by bio-inspired strategies that harness the design principles evolved by nature, to construct stimuli responsive and hierarchical materials in precise ways.[3,15–17]

The use of biomacromolecular building blocks to control the assembly of inorganic materials into user-specified and hierarchical assemblies is highly attractive because synthesis is conducted under mild conditions of temperature and pressure and environmentally-friendly solution conditions.[1,18,19] Yet, much

remains to be learnt in how to effectively design and use proteins and other biomolecules to fabricate materials with nanoscale precision and understand the mechanism of protein-guided materials synthesis.[1]

This work focuses on: (1) developing a greater understanding of how bifunctional silica-binding proteins may be designed and solution conditions chosen to control the pH-mediated assembly and disassembly of silica nanoparticles, and (2) setting the stage for the expansion of this approach to other solid-binding proteins, nanoparticle, and control mechanisms. More specifically, we build on previous work showing that a derivative of superfolder green fluorescent proteins (sfGFP) genetically modified with two oppositely located Car9 silica-binding peptides supports the repeated assembly (at pH 7.5) and disassembly (at pH 8.5) of 10 nm silica nanoparticles[20,21] to understand how mutations that reduce the binding affinity of the Car9 segments for silica – and their insertion location within the sfGFP framework – affect nanoparticle aggregation and dispersion. Moreover, we explore how small changes in pH and NaCl concentration affect aggregate assembly/disassembly, and construct, express, and, in some cases, purify *de novo* designed trimeric (1na0C3_3) and tetrameric (Ank1C4_2),[22] proteins modified with Car9 extensions at their C-terminus with the long-term goal of using these polypeptides to organize silica and Ni-NTA-coated nanoparticles into well-defined architectures.

## 1.1 Assembly of hybrid nanomaterials

Hybrid nanomaterials are molecular or colloidal-level combinations of organic and inorganic materials.[23,24] The emergent properties arising from the integration of organics and inorganics, and/or the unique functionalities of the constituent nanoparticle has driven interest in the development of such hybrid materials for a broad range of applications (**Fig. 1.1**).[23,24]

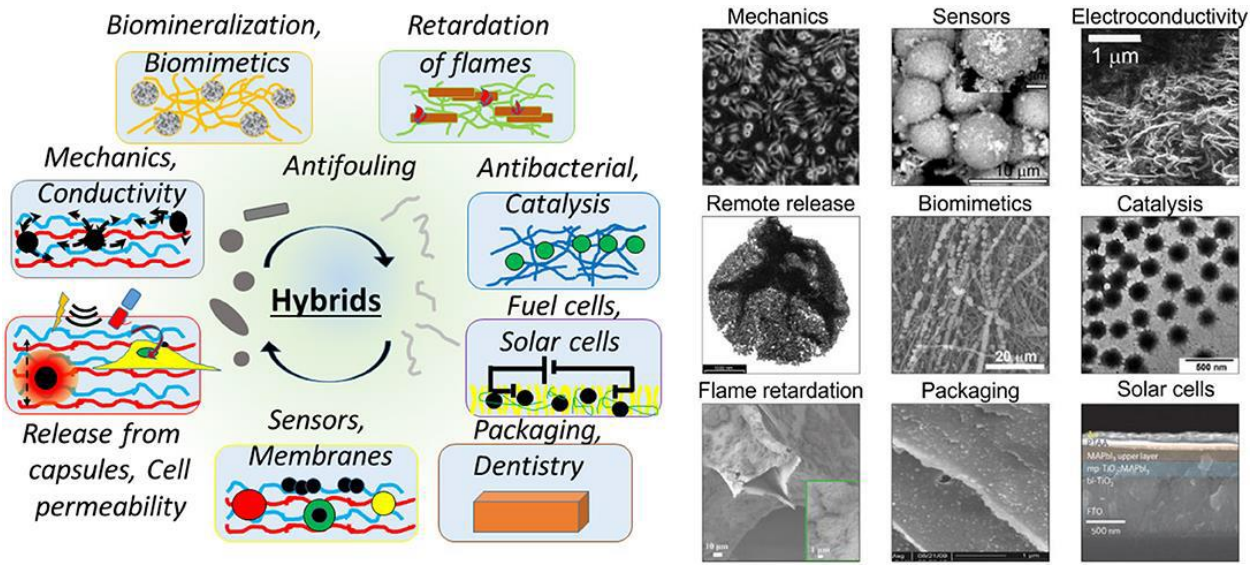


**Figure 1.1** Various applications of hybrid nanomaterials. Reproduced from Saveleva et al., 2019.[24]

Commonly used approaches for the production of hybrid nanomaterials include spontaneous colloidal crystallization,[25] physical wrapping,[26] chemical grafting,[27] guided assembly on patterned substrates,[28] assembly in emulsions,[29] and directed light- or magnetic field driven assembly.[30,31] Nanoparticles have also been connected using nucleic acids, polymers, ligands, and peptides as coupling agents.[12,32–36]

The grafting of DNA to nanoparticles (and especially gold nanoparticles, AuNPs) allows for temperature-dependent control of aggregation, with a dissociation stimulus that depends on the melting temperature of DNA bridges between bound particles.[36] DNA-bound nanoparticles can be assembled into soluble aggregates that are discrete, well-defined and, homogeneous,[37] or into nanocrystals with various lattice structures, symmetry, or size.[33,34,38] Although DNA has proven useful to program nanoparticle self-assembly and dispersion using temperature and light based dynamic control schemes,[18,39] the large-scale fabrication of these materials remains too costly and inefficient for practical use.

Polymer- and ligand-guided nanoparticle self-assembly has also been widely studied for the production of nanomaterials and thin films with varying degrees of control and reversibility.[40–43] The

aggregation of these materials mostly occurs through non-covalent forces, such as hydrophobic interactions, hydrogen bonding, and electrostatic interactions. While the destabilization of nanoparticles may occur due to the conjugation of the ligands and polymers to the surface, reversibility of nanoparticle assembly can be controlled to a certain extent by altering surface protonation/deprotonation using large pH shifts around the pKa.[42,44,45] Nevertheless, using these methods to conduct particle assembly is limited by both the magnitude and the length scale of the interactions, and the time scales can be an issue as well.[46,47]

Except DNA and polymers, a number of proteins and peptides are also utilized to develop new protein/peptide-based assemblies and related bionanomaterials.[3,48] One such examples includes the gold nanoparticle aggregation triggered via the adsorption of proteins, typically the lysozyme. Furthermore, the size of these protein-induced nanoparticle aggregation increases with the increase of protein concentration.[49,50] Based on the knowledge of these observations, more efforts were denoted to investigating the mechanism of protein-nanoparticle interactions and creating various types of bionanomaterials through the protein-nanoparticle aggregation, though these materials are typically static and the process still lacks dynamic control.[51]

## 1.2 Solid binding peptides and Car9

For decades, solid binding peptides (SBPs) have been used to investigate biotic-abiotic interactions and to organize organic and inorganic components for nanobiotechnology applications.[51] SBPs are short stretches of amino acids, typically 7 to 12 residues long that are isolated by phage or cell surface display.[3,14] They generally exhibit high selectivity and affinity for the surfaces of inorganic or organic materials and can be genetically fused to, or inserted within, larger protein frameworks to endow them with higher stability and solubility.[14] Furthermore, insertion of multiple SBPs within a single protein framework

provides an ability to bind or mineralize several inorganic components, and to build complex architectures that have been used for biomaterial production, nanostructure fabrication, and biomedical applications.[52–54]

Car9 is a dodecapeptide of amino acid sequence DSARGFKKPGKR that was isolated via FliTrx cell surface display by Baneyx group and was originally identified as a carbon-binding peptide exhibiting a preference for $sp^3$-hybridized carbon.[55,56] Car9 also binds to silica via electrostatic interaction. Surface plasmon resonance (SPR) experiments have shown that proteins incorporating the Car9 sequence exhibit sigmoidal adsorption sensorgrams on silica surfaces. This adhesion behavior can be captured using a two-step cooperative binding model.[57] Remarkably, substituting uncharged residues for some of the basic amino acids present in the Car9 sequence (e.g., K8AK11A) converts the binding modality from cooperative to one that can be captured by a standard Langmuir model.[57] A combination of experiments and simulations have revealed that the cooperative nature of silica binding is related to persistent interactions between a cluster of basic amino acids and the self-association of neighboring SBPs under conditions of high surface occupancy (**Fig. 1.2**).[58] Of note, Car9-silica interactions can be disrupted by supplementing the buffer with moderate concentrations of lysine or arginine.[58] This has enabled various practical applications such as affinity protein purification, microcontact printing, controlled protein release, and hybrid materials assembly.[56,59–62]

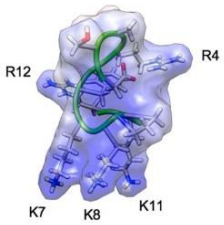


**Figure 1.2** Predicted low energy structure of the Car9 silica-binding peptide proposed by Rosetta. Reproduced from Hellner et al., 2020.[58]

Previous work performed in the Baneyx Lab[20,21] has shown that inserting the Car9 sequence at various locations of the sfGFP framework influences materials-binding properties (**Fig. 1.3**). Additionally, the solution pH was found to significantly influence the binding affinity of sfGFP-Car9 and its variants to silica, leading to the idea that variations in pH might be used to control the protein-mediated assembly and disassembly of silica nanostructures.[20,21]

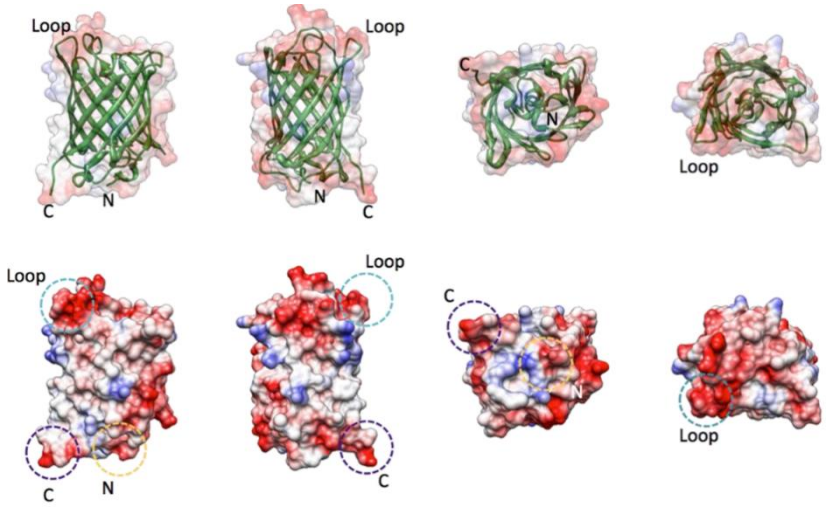


**Figure 1.3** Ribbon structures (top) of the sfGFP framework showing the locations of loop 9 (Loop) and of the amino- (N) and carboxy- (C) termini in front, back, bottom, and top orientations. Electrostatics are rendered on the molecular surface (bottom panel) between -10kTe (red) and +10kTe (blue). Reproduced from reference [21].

## 1.3 Silica surface chemistry and the absorption of peptides and proteins to silica nanoparticles

Silica, either in bulk or nanoparticulate form, has been used in catalysis, separations, biomedical applications, and pharmaceutical formulations due to its biocompatibility, low toxicity, stability, and large-scale synthetic availability.[63,64] Colloidal silica has also been used as a surfactant to improve the rheological properties of cosmetics and the delivery of drugs and genes.[65] Interactions between colloidal silica particles include Van der Waals attraction and electric double layer repulsions forces, as described by Derjaguin, Landau, Verwey, and Overbeek (DLVO) theory.[66,67]

In agreement with the Stern model, [68] the surface of silica particles is negatively charged at neutral pH due to the deprotonation of surface silanol groups. These silanols can exist as isolated silanols (≡Si−OH), geminal silanols (=Si(OH)2), or vicinal silanols (H-bonded silanols) depending on the materials crystal structure and synthesis method.[69] Under highly acidic conditions (pH ~2 to 4), silica particles have a zero net charge. According to electric double layer theory, addition of ions or salts shrinks the double layer surrounding the nanoparticles and leads to aggregation.[67,68] The valency of the counterions, nanoparticle concentration, and nanoparticle surface chemistry all influence aggregation propensity and rates.[67]

Although the kinetics and fundamentals of protein absorption on flat surfaces have been studied for decades, our understanding of protein absorption on nanoparticles is limited due to the complexity introduced by surface curvature.[70] Previous studies have shown that the adsorption of silica-binding peptides on silica nanoparticles is driven by multiple interactions including electrostatics and hydrophobic interactions, hydrogen bonding, ion-ion, ion-dipole, and Van der Waals interactions between the nanoparticles and the surface.[71,72] Additionally,

increasing in silica nanoparticle size and solution pH both result in increased surface ionization, leading to an increased number of silica-binding peptides bound to silica nanoparticles.[71]

## Chapter2. The sfGFP-SiNP system

### 2.1 Introduction

We previously reported on the display of SBPs with distinct materials specificity on opposite sides of the β-barrel of superfolder green fluorescent protein (sfGFP).[59,73] In these experiments, we made use of the sfGFP C-terminus and loop 9 -- a permissive location that tolerates the insertion of extraneous amino acids -- to respectively fuse or insert SBPs with different materials specificity. We utilized the resulting hetero-bifunctional solid-binding proteins to mineralize manganese-doped zinc sulfide nanocrystals and couple them to silica,[73] and to decorate carbon nanotubes with gold nanoparticles.[59] We also showed in preliminary studies,[20,21] that a homobifunctional variant of sfGFP containing the Car9 sequence at these two locations (thereafter referred to as sfGFP::Car9-Car9 with "::Car9" denoting an insertion within loop 9 and "-Car9" referring to a C-terminal fusion) can drive the assembly of 10 nm silica nanoparticles that encapsulate the dye rhodamine (RhSiNP). The resulting colloidal aggregates have an average hydrodynamic diameter ($D_h$) of ~ 1100 nm at pH 7.5. Remarkably, these aggregates can be dispersed into individual protein-coated nanoparticles and small clusters by shifting the solution pH to 8.5 (**Fig 2.1A**). The process is reversible for at least 3 cycles of pH changes as evidence by dynamic light scattering (DLS) measurements (**Fig. 2.4B**) and Förster Resonance Energy Transfer (FRET) experiments using the sfGFP chromophore as a donor and rhodamine as an acceptor (**Fig. 2.1D**). When a protein variant containing the K8AK11A substitutions within its C-terminal Car9 segment (sfGFP::Car9-K8AK11A) is used, the assemblies produced are about an order of magnitude smaller ($D_h$ ~120 nm) but cycles of disassembly and aggregation are still observed when the pH is cycled from 7.5 to 8.5 and back (**Fig. 2.1E**).

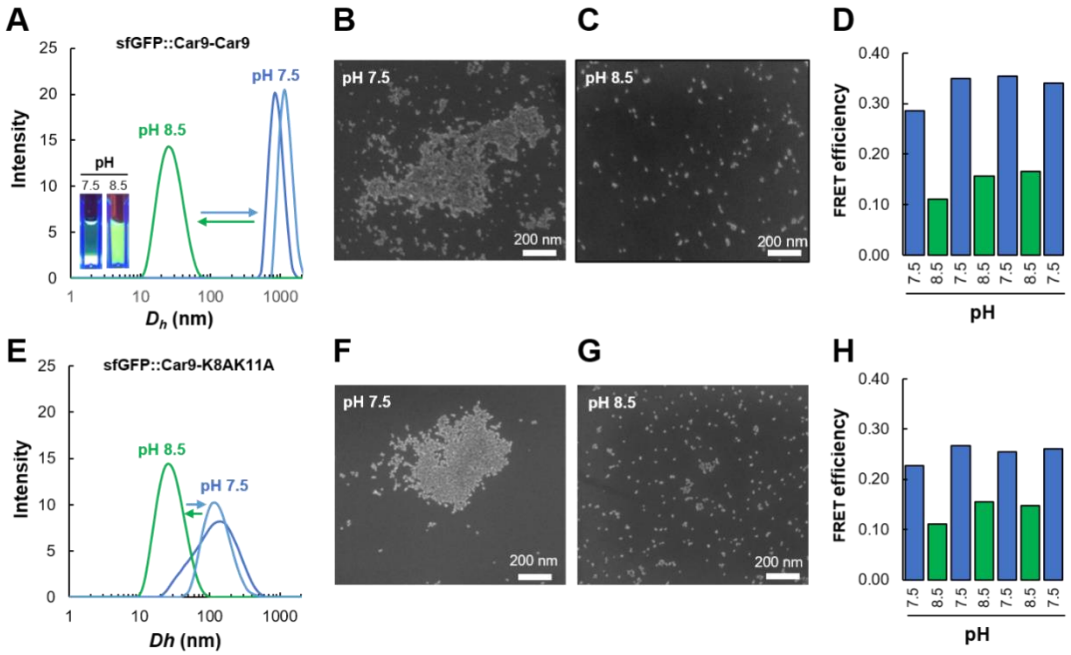


**Figure 2.1** pH-controlled assembly and dissociation of RhSiNP particles using sfGFP::Car9-Car9 (**A-D**) or sfGFP::Car9-K8AK11A (**E-H**). Size distributions were acquired by DLS after incubating 5 µM of sfGFP::Car-Car9 (**A**) or 5 µM of sfGFP::Car9-K8AK11A (**E**) with 1 µM RhSiNP for 30 minutes at pH 7.5 (dark blue traces), after adjusting the pH to 8.5 (green traces) and after returning the solution to pH 7.5 (light blue traces). The inset of panel A shows the appearance of the solution at pH 7.5 or 8.5 under UV illumination and after 30 min incubation without mixing. Aliquots of samples prepared at pH 7.5 (**B**, **F**) or pH 8.5 (**C**, **G**) were imaged by SEM. (**D**, **H**) FRET efficiencies were measured upon successive cycles of pH shifts. The figure is reproduced from reference [21].

Building on this work, we show here that is possible to tune the size of aggregates produced under near neutral conditions by: (1) introducing the K8AK11A mutations in the Car9 segment that is installed within loop 9; (2) using a Car9-sfGFP::Car9 variant in which Car9 sequences are present at the N-terminus and within loop 9 of sfGFP; and (3) adjusting the pH of the solution in small increments. We further show that the system's reversibility is limited by chemical fatigue associated with the accumulation of $Na^+$ ions that arises upon pH increase. We discuss the implications of these results for aggregate size tuning and dynamic switching.

## 2.2 Materials and Methods

### 2.2.1 DNA manipulations and protein purification

Plasmids pET24a(+)-sfGFP-Car9 and pET24a(+)-sfGFP::Car9 which encode derivatives of sfGFP modified with a Car9 sequence at the C-terminus or within loop 9 of the protein have been described.[56] Plasmids pET24a(+)-sfGFP::Car9-Car9 which encodes the dual-tagged protein sfGFP::Car9-Car9, was constructed by ligating a DNA cassette specifying the Car9 sequence into pET24a(+)-sfGFP digested with *BamHI* and *SpeI*.[57] Plasmid pET24a(+)-sfGFP::Car9-K8AK11A which encodes the dual-tagged protein sfGFP::Car9-K8AK11A, was constructed by ligating a DNA cassette encoding sfGFP::Car9 into pET24a(+)-sfGFP-K8K11A digested with *Kpn1* and *BsrG1*.[20] Plasmid pET24a(+)-sfGFP::K8AK11A-Car9 which encodes the dual-tagged protein sfGFP::K8AK11A-Car9 was constructed by site-directed mutagenesis of the Car9 sequence in loop 9 of sfGFP::Car9-Car9 to one containing the K8AK11A substitutions. Plasmid pET24a(+)-Car9-sfGFP::Car9 which encodes the dual-tagged protein Car9-sfGFP::Car9, was constructed by ligating a DNA cassette encoding Car9-sfGFP into pET24a(+)-sfGFP::Car9 digested with *NdeI* and *BsrGI*.[57] All constructs were verified by DNA sequencing and plasmids were introduced into *E. coli* BL21(DE3). Cultures were grown and induced, and proteins purified by silica affinity purification as described.[56,62] Purity was greater than 95% as judged by SDS-PAGE analysis of purified proteins (**Fig. A.1** in the appendix).

### 2.2.2 pH cycling for protein-NP solutions

Ten nm diameter silica nanoparticles terminated with native silanols and encapsulating the fluorescent dye rhodamine (RhSiNP) were purchased from Micromod Partikeltechnologie GmbH (Rostock, Germany) and possessed a concentration of 25 mg/mL. To assess the effect of pH on protein-mediated assembly or

disassembly, proteins and nanoparticle were mixed to a final concentration of 5 μM protein and 1 μM RhSiNP in 20 mM Tris-HCl, pH 7.5 in 1.5 mL Eppendorf tubes. The final volume was 1 mL. Tubes were wrapped in aluminum foil and rotated on a tube rotator for 30 minutes at room temperature before acquisition of DLS data. For pH cycling experiments, samples were first prepared in pH 7.5 buffer, as above, and supplied with 1M NaOH in 1 μL increments. The tube was inverted 10-16 times after each addition of base and the pH was measured with a Mettler Toledo microtip pH electrode. Once the solution reached pH 8.5, which took 8 μL of 1M NaOH for the first cycle and 10-15 μL for subsequent cycles, the tube was rotated for 30 minutes and DLS data acquired. To acidify the solution back to pH 7.5, 1M HCl was added in 1 μL increments and the pH monitored as above. Addition of 8 μL of acid was required for the first cycle and that of 10-14 μL for subsequent cycles. DLS data was acquired as above. The alkalinization and acidification processes add an average of 10 mM $Na^+$ or 10 mM $Cl^-$, respectively, to the system per cycle (**Table. A.1** in the appendix).

### 2.2.3 Dynamic Light Scattering.

Size distributions were acquired using a Zetasizer Nano ZS instrument (Malvern Instruments, U.K.) and size distributions data were extracted in terms of both intensity and number.

## 2.3 Results and Discussion

### 2.3.1 Chemical control of colloidal assembly with bifunctional solid-binding proteins: influence of SBP sequence and insertion location

Previously, our group used monovalent derivatives of sfGFP with a single Car9 silica-binding peptide genetically inserted either at the C-terminus (sfGFP-Car9) or within permissive loop 9 (sfGFP::Car9) of sfGFP to investigate how the local structure and electrostatics of the insertion point would influence

materials-binding properties. SPR was used to probe protein binding kinetics to silica-coated chips under two conditions of pH (7.5 and 8.5).[69,71,74] Rather counter-intuitively, these experiments revealed that an increase in pH, which should lead to the deprotonation of surface silanols and stronger surface adhesion of positively-charged Car9 segments, in fact reduced the binding of both proteins, with sfGFP::Car9 adhering more weakly to $SiO_2$ than sfGFP-Car9 at both pH.[57]

As depicted in **Fig. 2.1 A-D**, we previously exploited the availability of these two pH-addressable insertion locations to show that a bifunctional sfGFP::Car9-Car9 variant could drive the assembly of 10 nm RhSiNP at near neutral pH and that the aggregates could be repeatedly dispersed and re-aggregated by the simple expedient of toggling the pH between 7.5 and 8.5. We also found that replacing the C-terminal Car9 segment by a K8AK11A variant that binds more weakly to silica,[58] reduced the mean $D_h$ of the aggregates formed at pH 7.5 from 1100 ± 450 nm to 120 ± 60 nm, without affecting pH-mediated dissociation (**Fig. 2.1**).

Experiments conducted with freshly purified sfGFP::Car9-Car9 and sfGFP::Car9-K8AK11A variants, and a new batch of RhSiNP largely confirmed these results (**Fig. 2.2**). Aggregates produced at pH 7.5 using sfGFP::Car9-Car9 had a $D_h$ of 1200 ± 550 nm while those obtained with sfGFP::Car9-K8AK11A were 150 ± 88 nm in hydrodynamic diameter (**Fig. 2.2C**, green and red traces). Peaks were sharper and narrower when the sfGFP::Car9-K8AK11A intensity data was converted to numbers (**Table 2.1** and **Fig. 2.2E**), suggesting that a small number of large aggregates are the main contributors to the distribution's polydispersity. In both cases, and as expected, increasing the solution pH to 8.5 led to aggregate dispersion. The mean $D_h$ (24.4 ± 4.4 nm for sfGFP::Car9-Car9 and 23 ± 3.5 nm for sfGFP::Car9-K8AK11A) were consistent with the dimensions expected for 10-nm RhSiNP ($D_h$ = 16 nm at pH 8.5)[21] coated with a 4.5 nm

shell of protein. Nevertheless, a few large aggregates persisted in samples prepared with sfGFP::Car9-Car9 (**Fig 2.2C**). This is likely due to stronger adhesion forces between this protein and the particles relative to sfGFP::Car9-KA8K11A.

**Tabel 2.1** Mean $D_h$ and full width at half max (FWHM) of four different dual-tagged protein (5μM)-RhSiNP (1μM) aggregates in 20 mM Tris-HCl at pH 7.5 or 8.5.

| Protein | pH 7.5 | | | | pH 8.5 | | | |
|---|---|---|---|---|---|---|---|---|
| | Intensity | | Number | | Intensity | | Number | |
| | Mean $D_h$ | FWHM | Mean $D_h$ | FWHM | Mean $D_h$ | FWHM | Mean $D_h$ | FWHM |
| sfGFP::Car9-Car9 | 1200 | 1006 | 24.4 | 20.1 | 1180 | 880 | 24.1 | 17.6 |
| sfGFP::Car9-K8AK11A | 150 | 225 | 23.4 | 18.2 | 143 | 73 | 23 | 21.4 |
| sfGFP::K8AK11A-Car9 | 450 | 635 | 24.2 | 19.2 | 438 | 310 | 23.8 | 16.8 |
| Car9-sfGFP::Car9 | 620 | 505 | 23.8 | 18.4 | 615 | 298 | 23.8 | 15.7 |

To further investigate how SBP position and amino acid sequence would affect the outcomes of colloidal assembly, we constructed sfGFP::K8AK11A-Car9 in which the loop 9 insert contains the K8AK11A substitutions, and made use of Car9-sfGFP::Car9 which contains wild type Car9 segments at its N-terminus and within loop 9.[57] Not unexpectedly, both bifunctional proteins induced RhSiNP aggregation at pH 7.5 (**Fig. 2.2**). Car9-sfGFP-Car9 produced aggregates that were about 50% smaller than those obtained with sfGFP::Car9-Car9 ($D_h$ = 620 ± 250 nm; **Fig. 2.2B** orange and red traces), confirming a critical role of the C-terminal Car9 segment in the formation of large colloidal assemblies.

Consistent with this hypothesis, shifting the location of the K8AK11A mutation from the C-terminus to loop 9 led to an increase in aggregate size ($D_h$ = 450 ± 220 nm; **Fig. 2.2B** blue and green traces). As with sfGFP::Car9-K8AK11A, the distribution was fairly broad when scattering intensities were plotted as a function of $D_h$, but it could be sharpened by converting intensities to numbers (**Fig. 2.2C** and **2.2E**, green and blue traces). Adjusting the solution pH to 8.5 led to rather effective aggregate resolution, but a small number of aggregates persisted as in the case of all proteins containing a wild type Car9 sequence at their

C-termini (**Fig. 2.2C-D**).

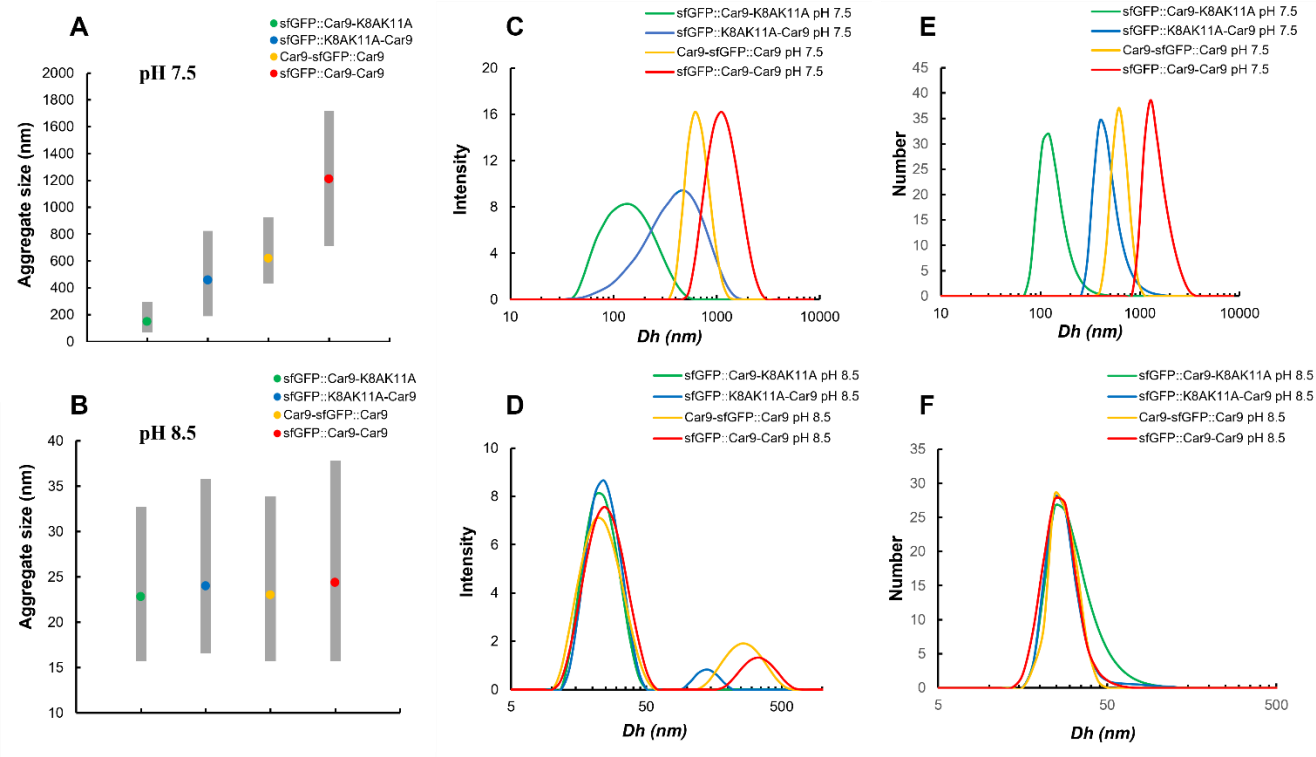


**Figure 2.2** Size distribution of dual-tagged proteins and 10nm RhSiNP in 20 mM Tris-HCl at pH 7.5 (A) and 8.5 (B). Panels C and D are size distributions in terms of scattering intensity at pH 7.5 and 8.5, respectively. Panels E and F show the size distribution in terms of number at pH 7.5 and 8.5, respectively. Grey error bars denote full width at half maximum to denote polydispersity of each average aggregate size.

To summarize, bifunctional silica-binding proteins can be used to assemble RhSiNPs into large supramolecular clusters at pH 7.5, and the size of these clusters can be controlled by the choice of the SBP insertion locations within the sfGFP framework, as well as the sequence of the SBPs. Increasing the pH by one unit resolves large assemblies into individual particles and alternating the pH between 7.5 and 8.5 supports repeated cycles of particle assembly and disassembly.

### 2.3.2 Controlling protein-NP aggregate size by modulating solution conditions.

An ability to precisely tune aggregate size is an important aspect of controlling and understanding the dynamical behavior of our system. Previous experiments conducted with sfGFP::Car9-Car9 and 10 nm

RhSiNP within the buffering range of Tris-HCl revealed that there was a sharp transition between dispersed and aggregated states when the pH was changed from 8.0 to 7.5 (**Fig. 2.3A**).[21] To expand on this knowledge, we conducted similar experiments using sfGFP::Car9-K8AK11A and sfGFP::K8AK11A-Car9 (**Fig. 2.3B-C**). All protein-induced assemblies showed a similar dependency on the solution pH. The largest aggregates were observed at neutral pH while hybrid assemblies were fully resolved into protein-decorated particles at pH 8.5. More excitingly, the two variants could be used to shift the response of the system towards more neutral pH and to access different size regimes in the 25 to 150 nm range by specifying the solution pH (Fig. 2.3B-C, insets and 2.3D). These results reflect a fine balance between the SBP-mediated adhesive forces that bring nanoparticles together and the electrostatic repulsive forces that keep them apart. That hybrid structures can be dispersed at pH 8.5 is consistent with the DLVO theory that predicts a decrease in zeta potential under more basic solution conditions, and therefore an increase on the stability of colloidal dispersions.[75,76] Indeed, we found that the zeta potential of "neat" RhSiNP were more negative (-34.9 ± 9.9 mV) at pH 8.5 than that (-24.7 ± 0.5 mV) at pH 7.5.

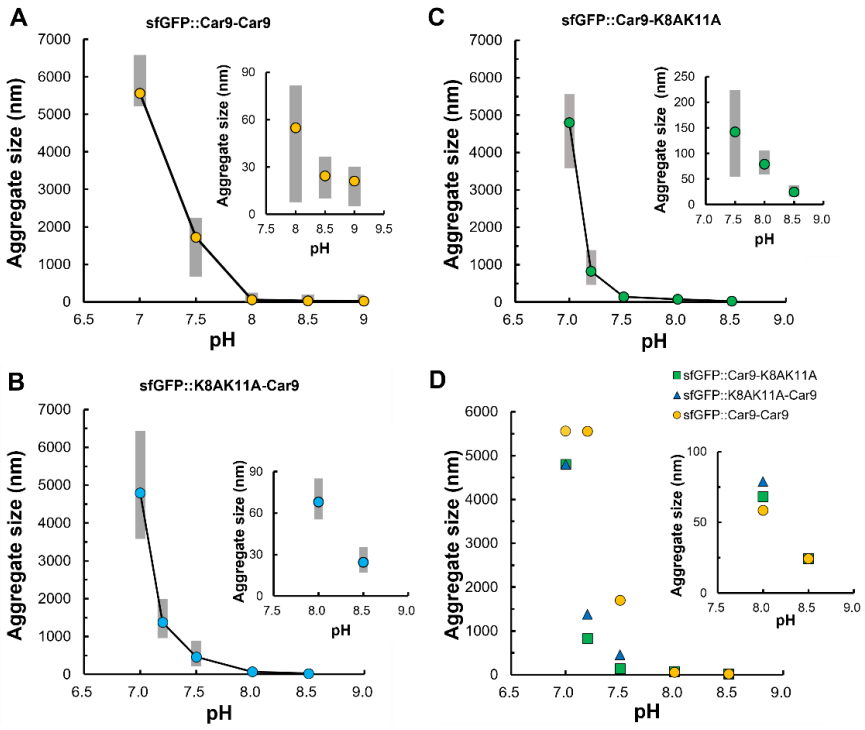


**Figure 2.3** Aggregate size obtained with the indicated proteins and 10 nm RhSiNP at the specified pH. The concentration of the RhSiNP was 1μM and that of protein 5μM. DLS data was collected in 20mM Tris-HCl, buffered at the indicated pH by addition of 1M NaOH or 1M HCl. (A) sfGFP::Car9-Car9, (B) sfGFP::Car9-K8AK11A,(C) sfGFP::K8AK11A-Car9. (D) Comparison of average aggregate sizes produced with the three different proteins. Panel A is courtesy of Julia Boese.

We next turned our attention to the influence of the buffer's ionic strength. The DLVO theory states that ions will shield surface charges, leading to a more positive zeta potential, and less stable colloidal suspensions or increased aggregation.[68] Initial experiments conducted by Julia Boese[21] showed that addition of NaCl to solutions containing a 5-fold molar excess of sfGFP::Car9-Car9 over 10 nm RhSiNP led to an increase in aggregate size at pH 7.5 (**Figure 2.4A**). A mean $D_h$ of ~4100 nm (which admittedly is at the dynamic range limit of our instrument) was observed after 30 min incubation for NaCl concentrations above 25 mM. This is much larger than the mean $D_h$ of 1700 nm size recorded in the absence of NaCl, and in agreement with the DLVO and double layer theories. More interestingly, addition of NaCl at pH 8.5, led to a progressive increase in cluster size, essentially negating the desirable pH-dependent particle dispersion

(**Figure 2.4A**). Because each cycle of alkalinization with NaOH adds about 10 mM of $Na^+$ ions to the solution, we sought to determine if the reversibility of assembly/dispersion might be limited by chemical fatigue associated with the accumulation of sodium ions. Indeed, **Fig. 2.4B** shows that when the concentration of carried over $Na^+$ reached ~40 mM, a situation that arises after four cycles of alkalinization, the protein-NP system lost its ability to undergo effective dispersion at pH 8.5. Of note, aggregate size started to increase at pH 7.5 as soon as $Na^+$ ions were added to the system (**Fig. 2.4B, C, E**). In addition, although there was a progressive loss in the ability to disperse particles with successive pH cycles (**Fig. 2.5. B, D, F**), conversion of scattering intensities to numbers revealed that about half of the particles were present in an isolated or small cluster form (**Fig. 2.5F**).

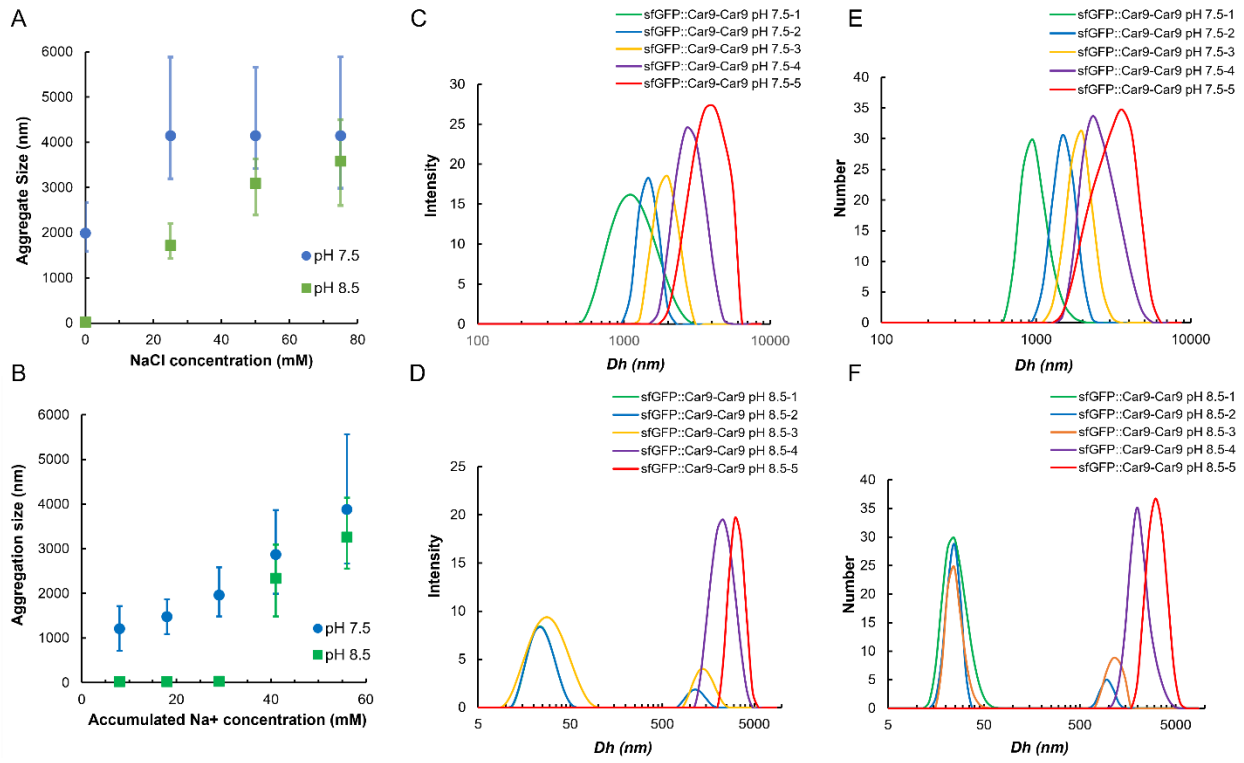


**Figure 2.4** Aggregate sizes produced by mixing sfGFP::Car9-Car9 and 10-nm RhSiNP at a 5:1 ratio at different imposed or carried over $Na^+$ concentrations. (A) Samples in 20mM Tris-HCl, pH 7.5 (Blue) or pH 8.5 (Green) were supplied with the indicated NaCl concentration and size distribution measured after 30 min incubation at room temperature. Mean $D_h$ are shown. Error bars correspond to the distributions' full width at half max and provide an indication of aggregate polydispersity. (B) Mean $D_h$ following 5 successive additions of NaOH for a 5:1 protein-nanoparticle solution initially prepared at pH 7.5. Cycling was conducted by adding 8-10µL of 1 M NaOH of 1 M HCl (see Methods for details). (C-F) Raw size distributions plotted in terms of scattering intensity (C, D) or converted to particle numbers (E,F) by the instrument's software. Panel A is courtesy of Julia Boese.

Overall, our date indicate that aggregation and disaggregation efficiency is significantly affected by altering the solution ionic strength during pH cycling. These findings can, on the other hand, be exploited by using the NaCl concentration to specify aggregate size. Considering that SBP insertion location and sequence also affect aggregation (**Fig. 2.2**), a rich parameter is available to control aggregate size and assembly-disassembly behavior. Theoretical treatment of the system should provide a mean to predictively choose these conditions for user-specified aggregation and disaggregation outcomes.

## 2.4 Conclusions and future direction

Motivated by the challenge of controlling the assembly of nanoscale materials in a precise and flexible fashion, we show that it is possible to use bifunctional solid binding proteins engineered with Car9 silica binding peptides to build a dynamic protein-nanoparticle system in which assembly/disassembly behavior is controlled by solution condition (e.g., pH and salt concentration) and protein design (e.g., SBP sequence and insertion point). The behavior of the system is underpinned by a fine balance between the adhesive forces associated with SBP-mediated protein-silica nanoparticles interactions and the repulsive electrostatic forces between negatively charged nanoparticles. In initial experiments, DLS, FRET and SEM were used to demonstrate that aggregates could be dispersed by a shift of one pH unit near the neutral value, and that the process was reversible for 3 cycles of pH shifts.[20,21]

In this work, we have further shown that high-affinity binding of RhSiNP through a C-terminal Car9 SBP is critical for the formation of large aggregates and that the size of the assemblies can be fine-tuned by weakening binding at the second site (e.g., by introducing the K8AK11A mutation in the loop 9 SBP or by moving it to the N-terminus of the protein). We have additionally demonstrated that a C-terminal K8AK11A mutation leads to the smallest aggregates and that the resulting panel of bifunctional silica-binding proteins can be used in conjunction with a judicious choice of the solution pH to specify aggregate size. While all hybrid assemblies can be repeatedly dispersed and aggregated by toggling the pH between 7.5 and 8.5, we have found that the progressive accumulation of $Na^+$ ions during successive cycles of alkalinization precludes full aggregate dissolution at the fourth cycle and beyond. These results are consistent with an observed increase in aggregate size at increasing NaCl concentrations at both pH 7.5 and 8.5. This behavior is well explained by the DLVO and electrical double layer theories for colloidal solutions and suggest that

NaCl aggregation can be used as an additional means to control aggregate size, albeit with loss of reversibility.

To avoid adding ions into the solution, we plan to use photoacids and photobases to tune the solution pH. This should allow for indefinite cycles of reversibility for the system. Moreover, we will use a recently developed rigid body model for the system to predictably determine the solution conditions and protein designs that give rise to precise aggregate sizes. Finally, we will make use of undecorated nanoparticle addition and PEG-modified bifunctional proteins to build structural diversity in the aggregates and expand the system's usefulness by making use of silica-coated semiconducting magic clusters and quantum dots. One of our long-term goals is to achieve dynamic control of nanoparticle assembly using computationally designed proteins. This will open up the next frontier for predictive production of hierarchical architectures useful in biomedicine, biomaterial fabrication and energy devices.

## Chapter3. *De novo* designed proteins

### 3.1 Introduction

Previously, we reported on the use of bifunctional derivatives of sfGFP incorporating Car9 SBPs to drive the assembly of RhSiNPs at pH 7.5 and showed that increasing the pH to 8.5 led to aggregate dispersion into protein-coated nanoparticles in a process that was reversible. We further showed that it was possible to control aggregate size by making use of a mutant silica-binding peptide (K8AK11A), by changing the location of these SBPs within the sfGFP framework, and by changing the solution pH and NaCl concentration. With the goal of organizing 10-nm RhSiNP nanoparticles into ordered assemblies, we turned our attention to the potential use of two oligomeric proteins computationally designed by Fallas et al.[22] whose size (~7x7-nm) matches the dimension of the nanoparticles and whose C-termini project in well-defined spatial directions (**Fig. 3.1**).

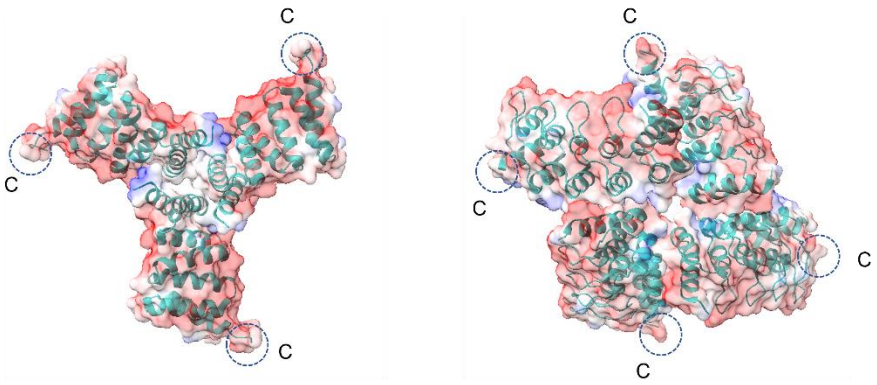


**Figure 3.1** Ribbon structures of the trimeric (1na0C3) and tetrameric (Ank1C4) protein frameworks showing the locations of carboxy- (C) termini.

Here, we use molecular biology to install silica-binding and hexahistidine extensions at the C-termini of two *de novo* designed proteins: a trimer named 1na0C3_3, and a tetramer named Ank1C4_1. We purify Ank1C4-His and use DLS to characterize its interaction with Ni-NTA-coated nanoparticles.

## 3.2 Materials and Methods

### 3.2.1 DNA manipulations and protein purification

G-blocks encoding 1na0C3_3 and Ank1C4_1 and including 20-30 bp overhangs were cloned into pET24a(+) through Gibson Assembly.[21] Plasmid pET24a(+)-1na0C3_3 encodes the trimer, 1na0C3_3, and plasmid pET24a(+)-Ank1C4_1 encodes the tetramer, Ank1C4_1. All constructs were verified by DNA sequencing and plasmids were introduced into *E. coli* BL21(DE3).

To build C-terminally His- and Car9-tagged versions of the proteins, DNA cassettes were ordered to create a *HindIII*, restriction site 5' of the *XhoI* restriction site via polymerase chain reaction (PCR). Next, DNA cassettes encoding a hexahistidne (His) or Car9 tag preceded by a GGGS linker were ligated between the *HindIII* and *XhoI* sites. Plasmid pET24a(+)-1na0C3_3-His and pET24a(+)-1na0C3_3-Car9 encode 1na0C3_3-His and 1na0C3_3-Car9, respectively. Plasmid pET24a(+)-Ank1C4_1-His and pET24a(+)-Ank1C4_1-Car9 encode Ank1C4_1-His and Ank1C4_1-Car9 respectively. All constructs (**Fig. A.3**) were verified by DNA sequencing and plasmids were introduced into *E. coli* BL21(DE3).

BL21(DE3) cells harboring pET24a(+)-1na0C3_3-Car9 or pET24a(+)-Ank1C4_1-Car9 were grown in 500 mL of LB medium at 37°C. Mid-exponential phase cells were induced with 1 mM IPTG and recombinant proteins allowed to accumulate overnight at room temperature. Attempts were made to purify Car9-tagged proteins by silica affinity chromatography as described.[56,62] His-tagged proteins were expressed as above and purified by Fast Protein Liquid Chromatography using a Ni-NTA column operated on BioRad NGC system. Proteins were loaded on a 5 mL column that was washed with 50 mL of buffer A (50 mM Tris-HCl, pH 7.5, 300 mM NaCl, 10 mM imidazole). Elution was conducted in a two-step process. First, 25 mL of 10% buffer B (50 mM Tris-HCl, pH 7.5, 300 mM NaCl, 200 mM imidazole) and 90% buffer

A was passed through the column. Second, 25 mL of 100% buffer B was run through the column. Proteins were collected in 5 mL of eluate and concentrated to ~10 μM in 20 mM Tris-HCl, pH 7.5 using Amplicon micron-concentrators. Aliquots (500 μL) were stored at -20°C and thawed before use.

### 3.2.2 Assembly of protein-NP solutions

Silica nanoparticles encapsulating rhodamine (RhSiNP) are described in Chapter 2. Ni-NTA-decorated gold nanoparticle 10 nm in diameter and at a concentration of $4.5 \times 10^{-8}$ M was purchased from Nanoprobes (New York, US). To assess the affinity of His-tagged proteins for Ni-NTA-gold nanoparticles (Ni-NTA AuNP), protein and nanoparticle were mixed at a final concentration of 0.45 μM protein and 0.045 μM Ni-NTA AuNP in 20mM Tris-HCl, pH 7.5. Samples (1 mL final volume) in 1.5 mL Eppendorf tubes covered with aluminum foil were mixed on a tube rotator for 30 minutes at room temperature before acquisition of DLS size distributions using a Zetasizer Nano ZS instrument (Malvern Instruments, U.K.).

## 3.3 Results and Discussion

### 3.3.1 Protein tagging and purification

The 1na0C3 and Ank1C4 *de novo*-designed proteins were modified with C-terminal His- and Car9-extensions with an intervening GGGS linker. We used standard Ni-NTA chromatography to purify the His-tagged proteins and silica affinity chromatography to purify Car9-tagged proteins. We successfully purified the Ank1C4-His tetramer (**Fig. 3.2**) SDS-PAGE analysis revealed clear bands corresponding to the 17.9-kDa protein[22] in the load (L) and second elution (E2) fractions.

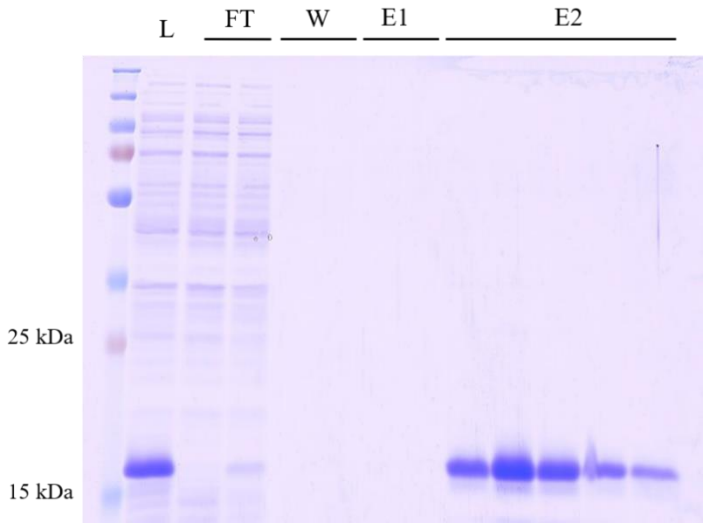


**Figure 3.2** Purification of Ank1C4-His. L: Load; FT: Flow through; W: Wash; E1: first elution; E2: second elution.

We tried to purify 1na0C3-His using the same protocol. Unfortunately, SDS-PAGE analysis (**Fig. A.4**) revealed that majority of the target protein (15.5-kDa band) eluted in the flow through. We attempted to increase the NaCl concentration in the wash and elution buffers to 1 M and increased the pH to 8.0 to strengthen in an effort to shield putative interactions between His tag and negatively charged region of the protein, and to enhance the binding of the His tag to the Ni-NTA column. These strategies were unsuccessful, and results were similar to those shown in **Fig. A.4**. We believe that our inability to purify 1na0C3-His is related to the inaccessibility of the tag.

We also attempted to purify Car9-tagged versions of the two proteins via silica chromatography. SDS-PAGE analysis (**Fig.A5-A6**) revealed that majority of these proteins eluted in flow through fractions. We conducted trials with silica gels of different sizes, but none improved binding. Although Car9-tagged Ank1C4 and 1na0C3 may have low affinity for silica, it is more likely that the Car9 extensions tags are not readily available for capture by the silica matric, and/or that local charge in the vicinity of the tag interferes with silica binding. To solve the above problems, we plan to build a longer linker between the proteins' C-termini and the His or Car9-tag

to improve accessibility. Additionally, we will attempt to identify other de novo-designed proteins with a more neutral surface charges to overcome potential tag confinement issues.

### 3.3.2 Attempted assembly of Ni-NTA AuNP using Ank1C4-His

Schreiber et al.[77] have used 10 nm AuNP with mixed tannic-citric acid ligands to assemble the ring-forming protein Hcp1 and its mutants into long chains where successive His-tagged protein oligomers are connected by AuNP. They also produced hedgehog-like structures by first decorating 40 nm AuNPs with Hcp1 mutants possessing three accessible cystine residues on the surface and growing protein chains from this central core by addition of 10 nm AuNPs and additional protein.[77] Ardini and coworkers[78] took advantage of the affinity of histidine residues for Ni-NTA functionalized gold nanoparticles to assemble the gold nanoparticles into one-dimensional nanotubes (~60 nm in length) with his-tagged peroxiredoxins. Inspired by these studies, we attempted to use Ank1C4-His to induce the assembly of 10 nm Ni-NTA AuNP into larger aggregates.

DLS analysis of purified Ank1C4-His revealed a $D_h$ of ~7 nm, which is consistent with the expected size of the tetramer[22] (**Fig. 3.3**, blue trace). Ni-NTA AuNP had a mean $D_h$ of ~ 14 nm that was consistent with the 10-nm size specified by the manufacturer (**Fig. 3.3**, red trace). However, we did not observe supramolecular assembly when Ni-NTA AuNP were mixed with purified Ank1C4-His at a 1:10 molar ratio as described by Schreiber and coworkers.[77] Rather, the mean $D_h$ of 22 nm was consistent with Ni-NTA AuNP decorated with Ank1C4-His. The precise reasons why the protein could not induce the assembly of the Ni-NTA AuNP remains unclear but may be related to an insufficient concentration of protein to overcome electrostatic repulsion between nanoparticles. Additionally, the large amounts of negative charges on the protein surface could interfere with the process. Additional work will be needed to probe these

possibilities.

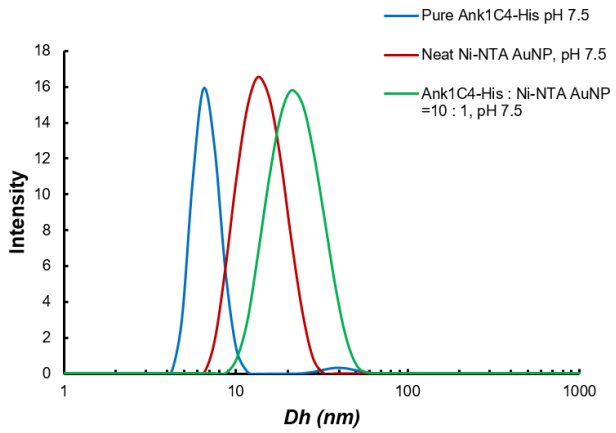


**Figure 3.3** Size distribution of pure Ank1C4-His (Blue), neat Ni-NTA AuNP (Dark red), and 0.45 μM Ank1C4-His mixed with 0.045 μM Ni-NTA AuNP (Green) in 20 mM Tris-HCl, pH 7.5.

## 3.4 Conclusions and future direction

Motivated by the challenge of controlling the assembly of nanoscale materials in a precise and flexible fashion, we constructed and attempted to purify oligomeric solid binding proteins tagged with the Car9 silica binding peptide. Preliminary attempts did not meet with success and additional work will be needed to optimize protein interaction with silica and to optimize the use of His-tagged proteins to assemble Ni-NTA AuNP.

## References


(1) Dickerson, M. B.; Sandhage, K. H.; Naik, R. R. Protein- and Peptide-Directed Syntheses of Inorganic Materials. *Chem. Rev.* **2008**, *108* (11), 4935–4978. https://doi.org/10.1021/cr8002328.

(2) Sarikaya, M.; Tamerler, C.; Schwartz, D. T.; Baneyx, F. Materials Assembly and Formation Using Engineered Polypeptides. *Annu. Rev. Mater. Res.* **2004**, *34* (1), 373–408. https://doi.org/10.1146/annurev.matsci.34.040203.121025.

(3) Sarikaya, M.; Tamerler, C.; Jen, A. K.-Y.; Schulten, K.; Baneyx, F. Molecular Biomimetics: Nanotechnology through Biology. *Nat. Mater.* **2003**, *2* (9), 577–585. https://doi.org/10.1038/nmat964.

(4) Ofir, Y.; Samanta, B.; Rotello, V. M. Polymer and Biopolymer Mediated Self-Assembly of Gold Nanoparticles. *Chem. Soc. Rev.* **2008**, *37* (9), 1814–1825. https://doi.org/10.1039/B712689C.

(5) Arole, D. V. M.; Munde, P. S. V. FABRICATION OF NANOMATERIALS BY TOP-DOWN AND BOTTOM-UP APPROACHES – AN OVERVIEW /paper/FABRICATION-OF-NANOMATERIALS-BY-TOP-DOWN-AND-%E2%80%93-AN-Arole-Munde/34f8921434fb256c9c8cca886722b5c920a1e4d2 (accessed Mar 31, 2021).

(6) DeFrates, K.; Markiewicz, T.; Gallo, P.; Rack, A.; Weyhmiller, A.; Jarmusik, B.; Hu, X. Protein Polymer-Based Nanoparticles: Fabrication and Medical Applications. *Int. J. Mol. Sci.* **2018**, *19* (6). https://doi.org/10.3390/ijms19061717.

(7) Rani, A.; Reddy, R.; Sharma, U.; Mukherjee, P.; Mishra, P.; Kuila, A.; Sim, L. C.; Saravanan, P. A Review on the Progress of Nanostructure Materials for Energy Harnessing and Environmental Remediation. *J. Nanostructure Chem.* **2018**, *8* (3), 255–291. https://doi.org/10.1007/s40097-018-0278-1.

(8) Zhao, H.; Sen, S.; Udayabhaskararao, T.; Sawczyk, M.; Kučanda, K.; Manna, D.; Kundu, P. K.; Lee, J.-W.; Král, P.; Klajn, R. Reversible Trapping and Reaction Acceleration within Dynamically Self-Assembling Nanoflasks. *Nat. Nanotechnol.* **2016**, *11* (1), 82–88. https://doi.org/10.1038/nnano.2015.256.

(9) Xia, Y.; Nguyen, T. D.; Yang, M.; Lee, B.; Santos, A.; Podsiadlo, P.; Tang, Z.; Glotzer, S. C.; Kotov, N. A. Self-Assembly of Self-Limiting Monodisperse Supraparticles from Polydisperse Nanoparticles. *Nat. Nanotechnol.* **2011**, *6* (9), 580–587. https://doi.org/10.1038/nnano.2011.121.

(10) Jia, G.; Sitt, A.; Hitin, G. B.; Hadar, I.; Bekenstein, Y.; Amit, Y.; Popov, I.; Banin, U. Couples of Colloidal Semiconductor Nanorods Formed by Self-Limited Assembly. *Nat. Mater.* **2014**, *13* (3), 301–307. https://doi.org/10.1038/nmat3867.

(11) Yi, C.; Liu, H.; Zhang, S.; Yang, Y.; Zhang, Y.; Lu, Z.; Kumacheva, E.; Nie, Z. Self-Limiting Directional Nanoparticle Bonding Governed by Reaction Stoichiometry. *Science* **2020**, *369* (6509), 1369–1374. https://doi.org/10.1126/science.aba8653.

(12) Boal, A. K.; Ilhan, F.; DeRouchey, J. E.; Thurn-Albrecht, T.; Russell, T. P.; Rotello, V. M. Self-Assembly of Nanoparticles into Structured Spherical and Network Aggregates. *Nature* **2000**, *404* (6779), 746–748. https://doi.org/10.1038/35008037.

(13) Mendes, A. C.; Baran, E. T.; Reis, R. L.; Azevedo, H. S. Self-Assembly in Nature: Using the Principles of Nature to Create Complex Nanobiomaterials. *WIREs Nanomedicine Nanobiotechnology* **2013**, *5* (6), 582–612. https://doi.org/10.1002/wnan.1238.

(14) Baneyx, F.; Schwartz, D. T. Selection and Analysis of Solid-Binding Peptides. *Curr. Opin. Biotechnol.* **2007**, *18* (4), 312–317. https://doi.org/10.1016/j.copbio.2007.04.008.

(15) Galusha, J. W.; Jorgensen, M. R.; Bartl, M. H. Diamond-Structured Titania Photonic-Bandgap

Crystals from Biological Templates. *Adv. Mater.* **2010**, *22* (1), 107–110. https://doi.org/10.1002/adma.200902852.
(16) Han, H.; Lee, J. Y.; Lu, X. Thermoresponsive Nanoparticles + Plasmonic Nanoparticles = Photoresponsive Heterodimers: Facile Synthesis and Sunlight-Induced Reversible Clustering. *Chem. Commun.* **2013**, *49* (55), 6122–6124. https://doi.org/10.1039/C3CC42273A.
(17) Schenkel, J. H.; Samanta, A.; Ravoo, B. J. Self-Assembly of Soft Hybrid Materials Directed by Light and a Magnetic Field. *Adv. Mater.* **2014**, *26* (7), 1076–1080. https://doi.org/10.1002/adma.201304689.
(18) Rogers, W. B.; Shih, W. M.; Manoharan, V. N. Using DNA to Program the Self-Assembly of Colloidal Nanoparticles and Microparticles. *Nat. Rev. Mater.* **2016**, *1* (3), 1–14. https://doi.org/10.1038/natrevmats.2016.8.
(19) Marichal, L.; Degrouard, J.; Gatin, A.; Raffray, N.; Aude, J.-C.; Boulard, Y.; Combet, S.; Cousin, F.; Hourdez, S.; Mary, J.; Renault, J.-P.; Pin, S. From Protein Corona to Colloidal Self-Assembly: The Importance of Protein Size in Protein–Nanoparticle Interactions. *Langmuir* **2020**, *36* (28), 8218–8230. https://doi.org/10.1021/acs.langmuir.0c01334.
(20) Zhao, Y. Stimuli-Responsive Assembly of Nanoparticles with Solid Binding Proteins, University of Washington, 2019.
(21) Boese, J. Exploiting the Interactions of Solid Binding Proteins with Silica to Form Colloidal Assemblies, University of Washington, 2020.
(22) Fallas, J. A.; Ueda, G.; Sheffler, W.; Nguyen, V.; McNamara, D. E.; Sankaran, B.; Pereira, J. H.; Parmeggiani, F.; Brunette, T. J.; Cascio, D.; Yeates, T. R.; Zwart, P.; Baker, D. Computational Design of Self-Assembling Cyclic Protein Homo-Oligomers. *Nat. Chem.* **2017**, *9* (4), 353–360. https://doi.org/10.1038/nchem.2673.
(23) Zhang, S.; Pelligra, C. I.; Feng, X.; Osuji, C. O. Directed Assembly of Hybrid Nanomaterials and Nanocomposites. *Adv. Mater.* **2018**, *30* (18), 1705794. https://doi.org/10.1002/adma.201705794.
(24) Saveleva, M. S.; Eftekhari, K.; Abalymov, A.; Douglas, T. E. L.; Volodkin, D.; Parakhonskiy, B. V.; Skirtach, A. G. Hierarchy of Hybrid Materials—The Place of Inorganics-in-Organics in It, Their Composition and Applications. *Front. Chem.* **2019**, *7*. https://doi.org/10.3389/fchem.2019.00179.
(25) van Blaaderen, A.; Ruel, R.; Wiltzius, P. Template-Directed Colloidal Crystallization. *Nature* **1997**, *385* (6614), 321–324. https://doi.org/10.1038/385321a0.
(26) Park, H. S.; Choi, B. G.; Hong, W. H.; Jang, S.-Y. Interfacial Interactions of Single-Walled Carbon Nanotube/Conjugated Block Copolymer Hybrids for Flexible Transparent Conductive Films. *J. Phys. Chem. C* **2012**, *116* (14), 7962–7967. https://doi.org/10.1021/jp209796f.
(27) Dayani, Y.; Malmstadt, N. Lipid Bilayers Covalently Anchored to Carbon Nanotubes. *Langmuir* **2012**, *28* (21), 8174–8182. https://doi.org/10.1021/la301094h.
(28) Nanomaterials Definition Matters. *Nat. Nanotechnol.* **2019**, *14* (3), 193–193. https://doi.org/10.1038/s41565-019-0412-3.
(29) Yi, G.-R.; Thorsen, T.; Manoharan, V. N.; Hwang, M.-J.; Jeon, S.-J.; Pine, D. J.; Quake, S. R.; Yang, S.-M. Generation of Uniform Colloidal Assemblies in Soft Microfluidic Devices. *Adv. Mater.* **2003**, *15* (15), 1300–1304. https://doi.org/10.1002/adma.200304890.
(30) Plunkett, K. N.; Mohraz, A.; Haasch, R. T.; Lewis, J. A.; Moore, J. S. Light-Regulated

Electrostatic Interactions in Colloidal Suspensions. *J. Am. Chem. Soc.* **2005**, *127* (42), 14574–14575. https://doi.org/10.1021/ja054666a.
(31) Ge, J.; Yin, Y. Magnetically Responsive Colloidal Photonic Crystals. *J. Mater. Chem.* **2008**, *18* (42), 5041–5045. https://doi.org/10.1039/B809958H.
(32) Hecht, F. M.; Bausch, A. R. Kinetically Guided Colloidal Structure Formation. *Proc. Natl. Acad. Sci.* **2016**, *113* (31), 8577–8582. https://doi.org/10.1073/pnas.1605114113.
(33) Macfarlane, R. J.; Lee, B.; Jones, M. R.; Harris, N.; Schatz, G. C.; Mirkin, C. A. Nanoparticle Superlattice Engineering with DNA. *Science* **2011**, *334* (6053), 204–208. https://doi.org/10.1126/science.1210493.
(34) Park, S. Y.; Lytton-Jean, A. K. R.; Lee, B.; Weigand, S.; Schatz, G. C.; Mirkin, C. A. DNA-Programmable Nanoparticle Crystallization. *Nature* **2008**, *451* (7178), 553–556. https://doi.org/10.1038/nature06508.
(35) Liu, Q.; Wang, H.; Shi, X.; Wang, Z.-G.; Ding, B. Self-Assembled DNA/Peptide-Based Nanoparticle Exhibiting Synergistic Enzymatic Activity. *ACS Nano* **2017**, *11* (7), 7251–7258. https://doi.org/10.1021/acsnano.7b03195.
(36) A DNA-based method for rationally assembling nanoparticles into macroscopic materials | Nature https://www.nature.com/articles/382607a0 (accessed Mar 31, 2021).
(37) Alivisatos, A. P.; Johnsson, K. P.; Peng, X.; Wilson, T. E.; Loweth, C. J.; Bruchez, M. P.; Schultz, P. G. Organization of "nanocrystal Molecules" Using DNA. *Nature* **1996**, *382* (6592), 609–611. https://doi.org/10.1038/382609a0.
(38) Biancaniello, P. L.; Kim, A. J.; Crocker, J. C. Colloidal Interactions and Self-Assembly Using DNA Hybridization. *Phys. Rev. Lett.* **2005**, *94* (5), 058302. https://doi.org/10.1103/PhysRevLett.94.058302.
(39) De Fazio, A. F.; El-Sagheer, A. H.; Kahn, J. S.; Nandhakumar, I.; Burton, M. R.; Brown, T.; Muskens, O. L.; Gang, O.; Kanaras, A. G. Light-Induced Reversible DNA Ligation of Gold Nanoparticle Superlattices. *ACS Nano* **2019**, *13* (5), 5771–5777. https://doi.org/10.1021/acsnano.9b01294.
(40) Cheng, G.; Xu, D.; Lu, Z.; Liu, K. Chiral Self-Assembly of Nanoparticles Induced by Polymers Synthesized via Reversible Addition–Fragmentation Chain Transfer Polymerization. *ACS Nano* **2019**, *13* (2), 1479–1489. https://doi.org/10.1021/acsnano.8b07151.
(41) Yi, C.; Yang, Y.; Liu, B.; He, J.; Nie, Z. Polymer-Guided Assembly of Inorganic Nanoparticles. *Chem. Soc. Rev.* **2020**, *49* (2), 465–508. https://doi.org/10.1039/C9CS00725C.
(42) Moaseri, E.; Bollinger, J. A.; Changalvaie, B.; Johnson, L.; Schroer, J.; Johnston, K. P.; Truskett, T. M. Reversible Self-Assembly of Glutathione-Coated Gold Nanoparticle Clusters via PH-Tunable Interactions. *Langmuir* **2017**, *33* (43), 12244–12253. https://doi.org/10.1021/acs.langmuir.7b02446.
(43) Zubair Iqbal, M.; Ali, I.; Khan, W. S.; Kong, X.; Dempsey, E. Reversible Self-Assembly of Gold Nanoparticles in Response to External Stimuli. *Mater. Des.* **2021**, *205*, 109694. https://doi.org/10.1016/j.matdes.2021.109694.
(44) Taladriz-Blanco, P.; Buurma, N. J.; Rodríguez-Lorenzo, L.; Pérez-Juste, J.; Liz-Marzán, L. M.; Hervés, P. Reversible Assembly of Metal Nanoparticles Induced by Penicillamine. Dynamic Formation of SERS Hot Spots. *J. Mater. Chem.* **2011**, *21* (42), 16880–16887. https://doi.org/10.1039/C1JM12175H.
(45) Cheng, L.; Liu, A.; Peng, S.; Duan, H. Responsive Plasmonic Assemblies of Amphiphilic

Nanocrystals at Oil−Water Interfaces. *ACS Nano* **2010**, *4* (10), 6098–6104. https://doi.org/10.1021/nn101685q.
(46) Li, F.; Josephson, D. P.; Stein, A. Colloidal Assembly: The Road from Particles to Colloidal Molecules and Crystals. *Angew. Chem. Int. Ed.* **2011**, *50* (2), 360–388. https://doi.org/10.1002/anie.201001451.
(47) Zhao, Y.; Thorkelsson, K.; Mastroianni, A. J.; Schilling, T.; Luther, J. M.; Rancatore, B. J.; Matsunaga, K.; Jinnai, H.; Wu, Y.; Poulsen, D.; Fréchet, J. M. J.; Paul Alivisatos, A.; Xu, T. Small-Molecule-Directed Nanoparticle Assembly towards Stimuli-Responsive Nanocomposites. *Nat. Mater.* **2009**, *8* (12), 979–985. https://doi.org/10.1038/nmat2565.
(48) Reddy, M. S. Biomineralization of Calcium Carbonates and Their Engineered Applications: A Review. *Front. Microbiol.* **2013**, *4*. https://doi.org/10.3389/fmicb.2013.00314.
(49) Dominguez-Medina, S.; Kisley, L.; Tauzin, L. J.; Hoggard, A.; Shuang, B.; D. S. Indrasekara, A. S.; Chen, S.; Wang, L.-Y.; Derry, P. J.; Liopo, A.; Zubarev, E. R.; Landes, C. F.; Link, S. Adsorption and Unfolding of a Single Protein Triggers Nanoparticle Aggregation. *ACS Nano* **2016**, *10* (2), 2103–2112. https://doi.org/10.1021/acsnano.5b06439.
(50) Zhang, D.; Neumann, O.; Wang, H.; Yuwono, V. M.; Barhoumi, A.; Perham, M.; Hartgerink, J. D.; Wittung-Stafshede, P.; Halas, N. J. Gold Nanoparticles Can Induce the Formation of Protein-Based Aggregates at Physiological PH. *Nano Lett.* **2009**, *9* (2), 666–671. https://doi.org/10.1021/nl803054h.
(51) Care, A.; Bergquist, P. L.; Sunna, A. Solid-Binding Peptides: Smart Tools for Nanobiotechnology. *Trends Biotechnol.* **2015**, *33* (5), 259–268. https://doi.org/10.1016/j.tibtech.2015.02.005.
(52) Chen, A. Y.; Deng, Z.; Billings, A. N.; Seker, U. O. S.; Lu, M. Y.; Citorik, R. J.; Zakeri, B.; Lu, T. K. Synthesis and Patterning of Tunable Multiscale Materials with Engineered Cells. *Nat. Mater.* **2014**, *13* (5), 515–523. https://doi.org/10.1038/nmat3912.
(53) Sano, K.-I.; Sasaki, H.; Shiba, K. Utilization of the Pleiotropy of a Peptidic Aptamer To Fabricate Heterogeneous Nanodot-Containing Multilayer Nanostructures. *J. Am. Chem. Soc.* **2006**, *128* (5), 1717–1722. https://doi.org/10.1021/ja057262r.
(54) Zhou, W.; Schwartz, D. T.; Baneyx, F. Single-Pot Biofabrication of Zinc Sulfide Immuno-Quantum Dots. *J. Am. Chem. Soc.* **2010**, *132* (13), 4731–4738. https://doi.org/10.1021/ja909406n.
(55) Coyle, B. L.; Rolandi, M.; Baneyx, F. Carbon-Binding Designer Proteins That Discriminate between Sp2- and Sp3-Hybridized Carbon Surfaces. *Langmuir* **2013**, *29* (15), 4839–4846. https://doi.org/10.1021/la4000846.
(56) Coyle, B. L.; Baneyx, F. A Cleavable Silica-Binding Affinity Tag for Rapid and Inexpensive Protein Purification. *Biotechnol. Bioeng.* **2014**, *111* (10), 2019–2026. https://doi.org/10.1002/bit.25257.
(57) Hellner, B.; Lee, S. B.; Subramaniam, A.; Subramanian, V. R.; Baneyx, F. Modeling the Cooperative Adsorption of Solid-Binding Proteins on Silica: Molecular Insights from Surface Plasmon Resonance Measurements. *Langmuir* **2019**, *35* (14), 5013–5020. https://doi.org/10.1021/acs.langmuir.9b00283.
(58) Hellner, B.; Alamdari, S.; Pyles, H.; Zhang, S.; Prakash, A.; Sprenger, K. G.; De Yoreo, J. J.; Baker, D.; Pfaendtner, J.; Baneyx, F. Sequence–Structure–Binding Relationships Reveal Adhesion Behavior of the Car9 Solid-Binding Peptide: An Integrated Experimental and Simulation Study. *J. Am.*

*Chem. Soc.* **2020**, *142* (5), 2355–2363. https://doi.org/10.1021/jacs.9b11617.
(59) Dunakey, S. J. G.; Coyle, B. L.; Thomas, A.; Xu, M.; Swift, B. J. F.; Baneyx, F. Selective Labeling and Decoration of the Ends and Sidewalls of Single-Walled Carbon Nanotubes Using Mono- and Bispecific Solid-Binding Fluorescent Proteins. *Bioconjug. Chem.* **2019**, *30* (3), 959–965. https://doi.org/10.1021/acs.bioconjchem.9b00097.
(60) Coyle, B. L.; Baneyx, F. Direct and Reversible Immobilization and Microcontact Printing of Functional Proteins on Glass Using a Genetically Appended Silica-Binding Tag. *Chem. Commun.* **2016**, *52* (43), 7001–7004. https://doi.org/10.1039/C6CC02660E.
(61) Yang, W.; Hellner, B.; Baneyx, F. Self-Immobilization of Car9 Fusion Proteins within High Surface Area Silica Sol–Gels and Dynamic Control of Protein Release. *Bioconjug. Chem.* **2016**, *27* (10), 2450–2459. https://doi.org/10.1021/acs.bioconjchem.6b00406.
(62) Soto-Rodríguez, J.; Coyle, B. L.; Samuelson, A.; Aravagiri, K.; Baneyx, F. Affinity Purification of Car9-Tagged Proteins on Silica Matrices: Optimization of a Rapid and Inexpensive Protein Purification Technology. *Protein Expr. Purif.* **2017**, *135*, 70–77. https://doi.org/10.1016/j.pep.2017.05.003.
(63) Hench, L. L. Bioceramics: From Concept to Clinic. *J. Am. Ceram. Soc.* **1991**, *74* (7), 1487–1510. https://doi.org/10.1111/j.1151-2916.1991.tb07132.x.
(64) Kresge, C. T.; Leonowicz, M. E.; Roth, W. J.; Vartuli, J. C.; Beck, J. S. Ordered Mesoporous Molecular Sieves Synthesized by a Liquid-Crystal Template Mechanism. *Nature* **1992**, *359* (6397), 710–712. https://doi.org/10.1038/359710a0.
(65) Wang, M.; Marepally, S. K.; Vemula, P. K.; Xu, C. Chapter 5 - Inorganic Nanoparticles for Transdermal Drug Delivery and Topical Application. In *Nanoscience in Dermatology*; Hamblin, M. R., Avci, P., Prow, T. W., Eds.; Academic Press: Boston, 2016; pp 57–72. https://doi.org/10.1016/B978-0-12-802926-8.00005-7.
(66) Berg, J. C. *An Introduction to Interfaces and Colloids: The Bridge to Nanoscience*; WORLD SCIENTIFIC, 2009. https://doi.org/10.1142/7579.
(67) Verwey, E. J. W. Theory of the Stability of Lyophobic Colloids. *J. Phys. Colloid Chem.* **1947**, *51* (3), 631–636. https://doi.org/10.1021/j150453a001.
(68) Kobayashi, M.; Juillerat, F.; Galletto, P.; Bowen, P.; Borkovec, M. Aggregation and Charging of Colloidal Silica Particles: Effect of Particle Size. *Langmuir* **2005**, *21* (13), 5761–5769. https://doi.org/10.1021/la046829z.
(69) Parida, S. K.; Dash, S.; Patel, S.; Mishra, B. K. Adsorption of Organic Molecules on Silica Surface. *Adv. Colloid Interface Sci.* **2006**, *121* (1), 77–110. https://doi.org/10.1016/j.cis.2006.05.028.
(70) Wu, X.; Narsimhan, G. Effect of Surface Concentration on Secondary and Tertiary Conformational Changes of Lysozyme Adsorbed on Silica Nanoparticles. *Biochim. Biophys. Acta BBA - Proteins Proteomics* **2008**, *1784* (11), 1694–1701. https://doi.org/10.1016/j.bbapap.2008.06.008.
(71) Puddu, V.; Perry, C. C. Interactions at the Silica–Peptide Interface: The Influence of Particle Size and Surface Functionality. *Langmuir* **2014**, *30* (1), 227–233. https://doi.org/10.1021/la403242f.
(72) Puddu, V.; Perry, C. C. Peptide Adsorption on Silica Nanoparticles: Evidence of Hydrophobic Interactions. *ACS Nano* **2012**, *6* (7), 6356–6363. https://doi.org/10.1021/nn301866q.
(73) Swift, B. J. F.; Shadish, J. A.; DeForest, C. A.; Baneyx, F. Streamlined Synthesis and Assembly of a Hybrid Sensing Architecture with Solid Binding Proteins and Click Chemistry. *J. Am. Chem. Soc.*

**2017**, *139* (11), 3958–3961. https://doi.org/10.1021/jacs.7b00519.
(74) Lowe, B. M.; Skylaris, C.-K.; Green, N. G. Acid-Base Dissociation Mechanisms and Energetics at the Silica–Water Interface: An Activationless Process. *J. Colloid Interface Sci.* **2015**, *451*, 231–244. https://doi.org/10.1016/j.jcis.2015.01.094.
(75) Bhattacharjee, S. DLS and Zeta Potential – What They Are and What They Are Not? *J. Controlled Release* **2016**, *235*, 337–351. https://doi.org/10.1016/j.jconrel.2016.06.017.
(76) Friday; February 1; Share, 2013. An Overview of the Zeta Potential - Part 1: The Concept http://www.americanpharmaceuticalreview.com/Featured-Articles/133232-An-Overview-of-the-Zeta-Potential-Part-1-The-Concept/ (accessed May 1, 2021).
(77) Schreiber, A.; Huber, M. C.; Cölfen, H.; Schiller, S. M. Molecular Protein Adaptor with Genetically Encoded Interaction Sites Guiding the Hierarchical Assembly of Plasmonically Active Nanoparticle Architectures. *Nat. Commun.* **2015**, *6* (1), 6705. https://doi.org/10.1038/ncomms7705.
(78) Ardini, M.; Giansanti, F.; Leandro, L. D.; Pitari, G.; Cimini, A.; Ottaviano, L.; Donarelli, M.; Santucci, S.; Angelucci, F.; Ippoliti, R. Metal-Induced Self-Assembly of Peroxiredoxin as a Tool for Sorting Ultrasmall Gold Nanoparticles into One-Dimensional Clusters. *Nanoscale* **2014**, *6* (14), 8052–8061. https://doi.org/10.1039/C4NR01526F.

## Appendix A. Supplementary Information for Chapter 2

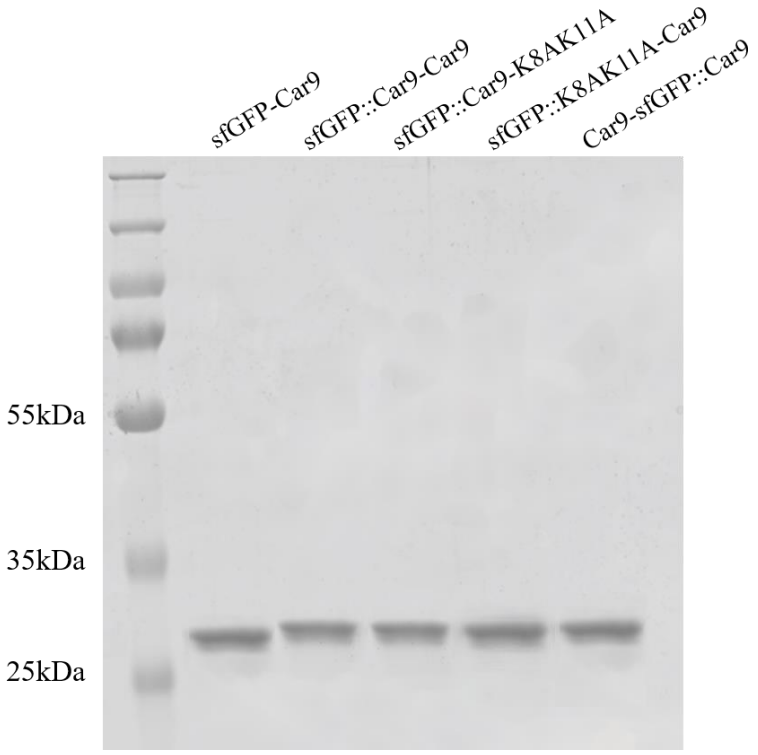


**Figure A.1** SDS-Page gel of dual-tagged sfGFP with Car9 and Car9 variant K8AK11A in different locations and use sfGFP-Car9 as a control.

**Table A.1** The volume of 1M NaOH/HCl and accumulated $Na^+$ concentration.
Note: the number after the dash represents the number of times this solution pH reaches.

| pH | The volume of 1M NaOH/HCl added in the solution (μL) | Accumulated $Na^+$ concentration (mM) |
|---|---|---|
| 8.5-1 | 8 | 8 |
| 7.5-2 | 8 | |
| 8.5-2 | 10 | 18 |
| 7.5-3 | 10 | |
| 8.5-3 | 11 | 29 |
| 7.5-4 | 12 | |
| 8.5-4 | 12 | 41 |
| 7.5-5 | 14 | |
| 8.5-5 | 15 | 56 |

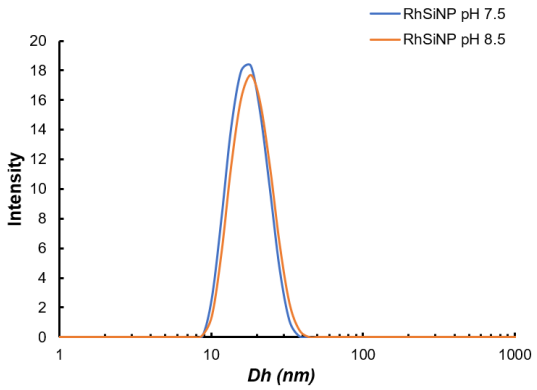


**Figure A.2** Size distribution of pure 10nm RhSiNP in 20 mM Tris-HCl at pH 7.5 (blue) and 8.5 (orange).

## Supplementary Information for Chapter 3

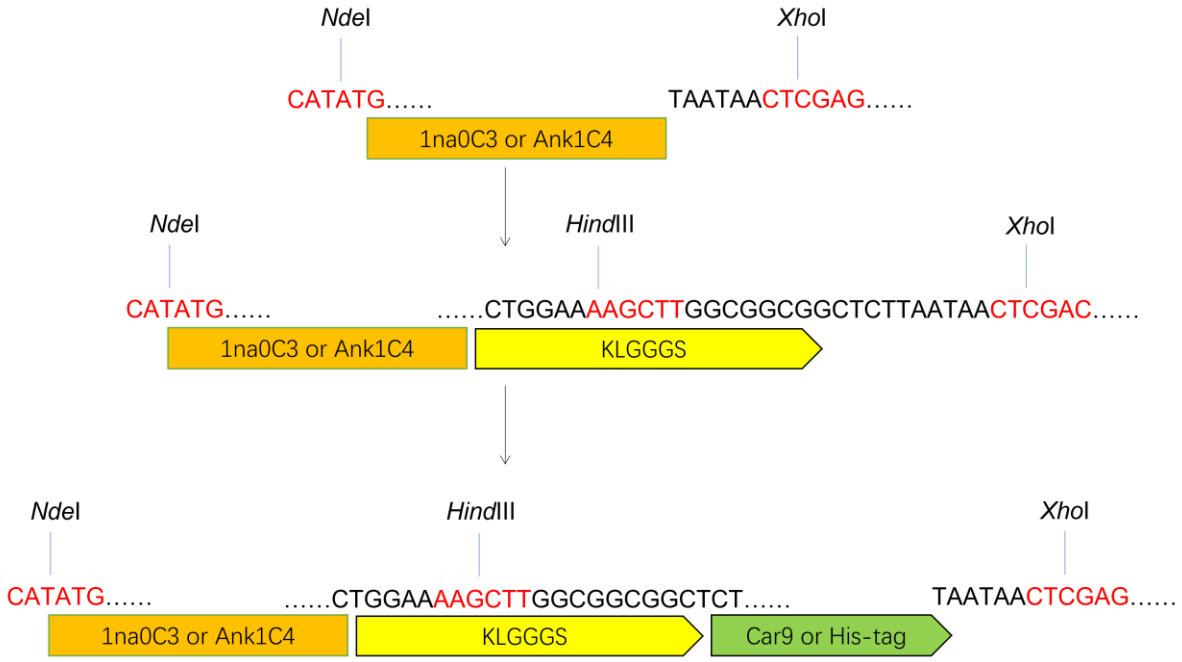


**Figure A.3** Scheme of protein construction. The restriction sites are labeled with red.

DNA Sequences used to make proteins in Chapter 3. Capital letters represent the sequence of the expressed protein and the lowercase letter represent the Gibson overlaps as well as any fragments not expressed as a protein.

1na0C3-His:

taactttaagaaggagatatacatATGAACCTGGCGGAAAAAATGTACAAGGCCGGTAACGCGATGTACCGT

AAAGGCCAGTACACCATTGCGATCATCGCTTACACCCTGGCACTGCTGAAGGATCCGAATAAC

GCAGAGGCTTGGTATAACCTGGGCAACGCGGCGTACAAAAAAGGTGAATACGATGAAGCCAT

TGAAGCATACCAGAAAGCGCTTGAACTGGATCCGAACAACGCGGAAGCGTGGTACAATCTGG

GTAACGCCTACTACAAGCAGGGCGATTACGACGAAGCCATCGAATACTACCAGAAAGCGCTG

GAACTCGACCCGAACAACGCAGAAGCTAAACAGAACCTGGGTAACGCTAAGCAGAAACAGG

GCCTGGAAAAGCTTGGCGGCGGCTCTcaccaccaccaccaccactaataactcgagcaccaccaccaccaccactga

1na0C3-Car9:

taactttaagaaggagatatacatATGAACCTGGCGGAAAAAATGTACAAGGCCGGTAACGCGATGTACCGT
AAAGGCCAGTACACCATTGCGATCATCGCTTACACCCTGGCACTGCTGAAGGATCCGAATAAC
GCAGAGGCTTGGTATAACCTGGGCAACGCGGCGTACAAAAAAGGTGAATACGATGAAGCCAT
TGAAGCATACCAGAAAGCGCTTGAACTGGATCCGAACAACGCGGAAGCGTGGTACAATCTGG
GTAACGCCTACTACAAGCAGGGCGATTACGACGAAGCCATCGAATACTACCAGAAAGCGCTG
GAACTCGACCCGAACAACGCAGAAGCTAAACAGAACCTGGGTAACGCTAAGCAGAAACAGG
GCCTGGAAAAGCTTGGCGGCGGCTCTGACAGTGCTCGCGGGTTTAAAAAGCCTGGGAAGCG
Gtaataactcgagcaccaccaccaccaccactga

Ank1C4-His:

taactttaagaaggagatatacatATGTCTGAAGATGGTGAACTGCTGATTCTGGCTGCGGAACTGGGTATT
GCAGAAGCTGTACGCATGCTGATCGAACAGGGCGCCGACGTTAACGCTTCCGACGATGACG
GTCGCACTCCGCTTCACCATGCTGCGGAAAACGGCCATCTGGCTGTAGTGCTGCTTCTGCTG
CTGAAAGGCGCGGATGTGAACGCTAAAGATTCTGACGGCCGTACTCCGCTGCATCATGCTGC
TGAAAACGGTCACAAAACCGTTGTTCTGCTTCTTATCCTGATGGGTGCTGATGTTAACGCTA
AGGATTCCGATGGCCGCACCCCGCTTCACCACGCGGCGGAAAACGGTCATAAAGAAGTGGT
TAAACTGCTGATTCGCAAGGGCGCAGACGTTAACACCTCTGACTCGGACGGTCGTACTCCGC
TTGATCTGGCCCGTGAACATGGCAACGAAGAAGTTGTTAAACTGCTGGAAAAACAGCTGGA
AAAGCTTGGCGGCGGCTCTcaccaccaccaccaccactaataactcgagcaccaccaccaccaccactga

Ank1C4-Car9:

taactttaagaaggagatatacatATGTCTGAAGATGGTGAACTGCTGATTCTGGCTGCGGAACTGGGTATTG
CAGAAGCTGTACGCATGCTGATCGAACAGGGCGCCGACGTTAACGCTTCCGACGATGACGGT

CGCACTCCGCTTCACCATGCTGCGGAAAACGGCCATCTGGCTGTAGTGCTGCTTCTGCTGCTG
AAAGGCGCGGATGTGAACGCTAAAGATTCTGACGGCCGTACTCCGCTGCATCATGCTGCTGA
AAACGGTCACAAAACCGTTGTTCTGCTTCTTATCCTGATGGGTGCTGATGTTAACGCTAAGGA
TTCCGATGGCCGCACCCCGCTTCACCACGCGGCGGAAAACGGTCATAAAGAAGTGGTTAAAC
TGCTGATTCGCAAGGGCGCAGACGTTAACACCTCTGACTCGGACGGTCGTACTCCGCTTGATC
TGGCCCGTGAACATGGCAACGAAGAAGTTGTTAAACTGCTGGAAAAACAGCTGGAAAAGCT
TGGCGGCGGCTCTGACAGTGCTCGCGGGTTTAAAAAGCCTGGGAAGCGGtaataactcgagcaccacca
ccaccaccactga

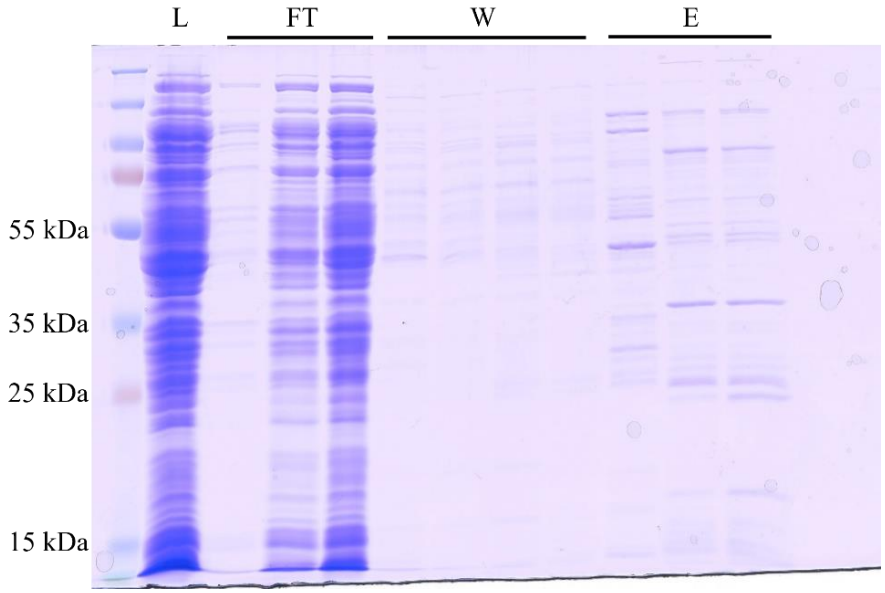


**Figure A.4** Purification of 1na0C3-His. L: Load; FT: Flow through; W: Wash; E: Elution.

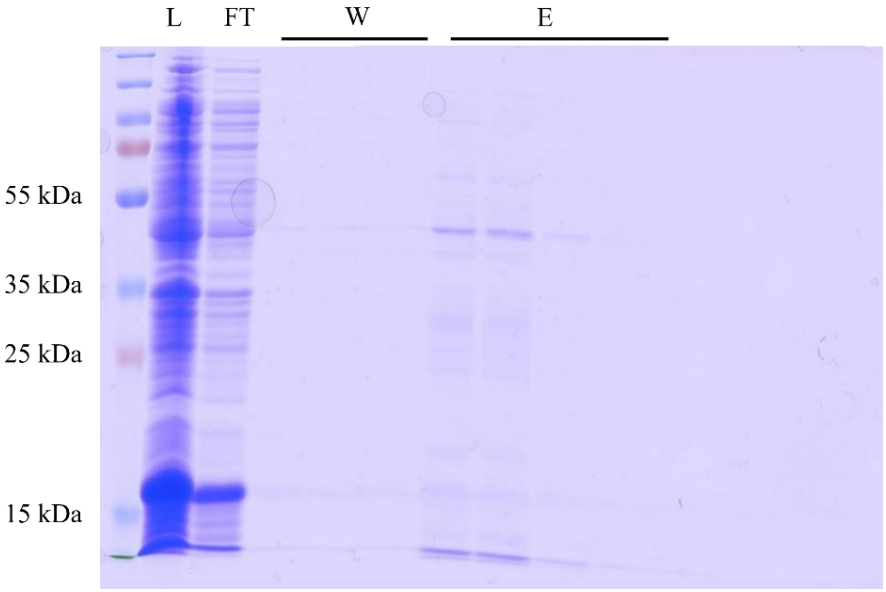


**Figure A.5** Purification of Ank1C4-Car9. L: Load; FT: Flow through; W: Wash; E: Elution.

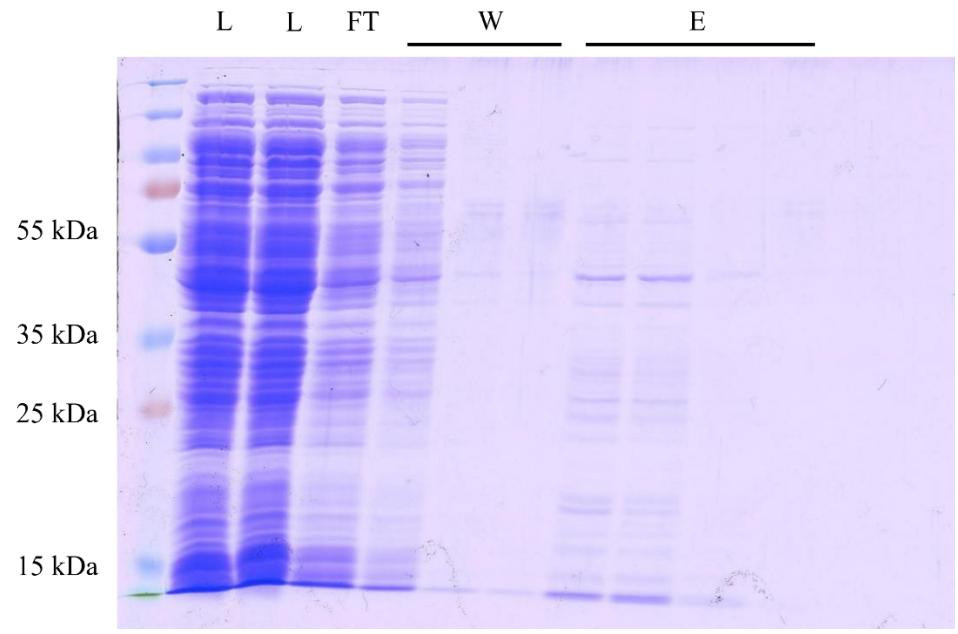


**Figure A.6** Purification of 1na0C3-Car9. L: Load; FT: Flow through; W: Wash; E: Elution. The two load lanes exist due to the misloading.